Received: 23 November 2020 | Revised: 25 June 2021 | Accepted: 3 July 2021

DOI: 10.1002/met.2017

RESEARCH ARTICLE

Meteorological Applications
Science and Technology for Weather and Climate

Comprehensive physics testing and adaptive weather research and forecasting physics for day-ahead solar forecasting

Robert Huva[1] | **Guiting Song**[1] | **Xiaohui Zhong**[1] | **Yangyang Zhao**[2]

[1]Envision Digital International Pte Ltd, Singapore, Singapore

[2]Envision Energy Pte Ltd, Shanghai, China

Correspondence
Guiting Song, Envision Digital International Pte Ltd, Singapore, Singapore.
Email: guiting.song@envision-digital.com

Funding information
Envision Digital Singapore

Abstract

Numerical weather prediction (NWP) models, which attempt to simulate the full state of the atmosphere, come with many options for dealing with processes that are unable to be explicitly resolved by the model. These model parameterizations are an ongoing area of research in atmospheric science. However, with continuous contributions from the research community and subsequent upgrade of the NWP codes, there are often many options for each unresolved process—leaving the user confronted with potentially thousands of ways to configure the model. We use the weather research and forecasting (WRF) model to forecast global horizontal irradiance (GHI) and undertake the task of narrowing down these options for a location in Qinghai, China. We show that optimizing the configuration of the WRF model based on the type of day (sunny, partly cloudy, or cloudy) is 13.6% better than using a single best configuration for all types of days. We also show that this performance improvement holds true for a longer 3-month test period (17.8% improvement).

KEYWORDS

irradiance forecasting, NWP, optimization

1 | INTRODUCTION

Solar continues to be the fastest growing renewable technology in the world with an annual average growth rate of over 40% from 2000 to 2018 for the Organisation for Economic Co-operation and Development (OECD) (IEA, 2019). Many countries across the world now have non-trivial amounts of variable supply in their electricity mix (IEA, 2019). Various strategies have been employed to deal with the unknown output from such sources of electricity as solar. In China and India, the grid operators require wind and solar farm operators to forecast their output for the coming hours or days. Penalties are then imposed for operators who cannot meet the accuracy requirements (China GB/T 19964-2012, n.d.; Mitra et al., 2016). In other countries, like Australia, the grid operators undertake the task of forecasting the output from wind and solar in order to stabilize the grid (AEMO, 2020). Under both scenarios, the impact from an incorrect forecast can be significant—either financially or in terms of grid stability. Research on how to best forecast solar, or wind, is thus a burgeoning field.

To forecast solar irradiance, there are a variety of techniques that are commonly used (Ahmed et al., 2020).

These techniques range from statistical models, to physical models and combinations thereof depending on the location and the forecast horizon. At time horizons beyond a few hours, techniques that incorporate numerical weather prediction (NWP) output are generally accepted as best practice (Huang & Thatcher, 2017). Reasons for the deterioration in performance of statistical models centre on the chaotic nature of the atmosphere and the role of clouds in modulating the irradiance time series. Under partly cloudy or cloudy conditions, the irradiance time series can exhibit very little autocorrelation. During times of cloudiness, or at longer time horizons, NWP models can out-perform statistical techniques due to their ability to simulate the processes that form clouds. NWP models operate by discretizing the atmosphere across a 3D grid and stepping forward the governing equations using polynomial expansion. Starting from an initial guess, NWP models are able to give a complete picture of the state of the atmosphere at some time later.

The weather research and forecasting (WRF) model is a commonly used NWP model for local NWP forecasting (Skamarock & Klemp, 2008). WRF is a community-based model that undergoes a major update every year. Each major release incorporates new advancements in the field of NWP, which in recent years has also included options specific to solar forecasting (Jimenez et al., 2016). The use of NWP models, like WRF, for forecasting irradiance at the local scale is an ever-growing area of research. At forecast horizons beyond 12 h, there are numerous studies from countries with various climates to show the importance of NWP in forecasting irradiance. In the mid-latitudes, this includes studies from Greece (Zempila et al., 2016), the United States (Larson et al., 2016) and Japan (Murata et al., 2018), while countries at more tropical latitudes include studies from Reunion Island (Diagne et al., 2014) and Singapore (Verbois et al., 2018). The region of concern for the present study, Qinghai, China, is mid-latitude and largely at high elevation. The climate of the Qinghai region exhibits seasonal variability that includes surface temperatures well below 0°C in the winter and warm, mostly dry, conditions in the summer. Che et al. (2019) studied the use of the WRF model for forecasting irradiance in Qinghai, China. The authors found variation in the performance of WRF based on season as well as the cloud amount. Duan et al. (2018) also studied biases in surface variables using WRF over northwest China, including Qinghai. The authors found summertime biases in 2-m temperature and 10-m wind speed that correlated with terrain height. Song et al. (2019) analysed the effects of atmospheric aerosols on radiative forcing and discussed the impact on surface short- and long-wave fluxes for eastern China using the Rapid Radiative Transfer Model (RRTMG) model within WRF. The authors found that an increase in aerosol loading during the summer months of 2002–2008 led to smaller cloud droplet size along with net cooling and a decrease in radiative forcing at the surface.

The reason for biases or large error by models like WRF can be traced back to many different causes depending on the variable and location being studied. Broadly speaking, the WRF model, like all NWP, suffers from error spreading due to three main sources: sub-grid scale processes not captured by the resolution of the model, complex processes that require too much computation to be resolved explicitly, and errors in the initial state of the model. The first two error sources can be partly addressed through model parameterizations—like the radiative transfer model (RTM) or microphysics schemes. The parameterizations attempt to mimic the behaviour of a specific process and can feed the result of this behaviour back to the model. Thus, one approach for reducing model error is to choose a set of parameterizations that best resolves the processes important to each study.

The aforementioned Che et al. (2019) study tested multiple RTM options for their Qinghai site and found the Dudhia scheme to work best over two separate seasons. Zhang et al. (2018) also studied northwest China, analysing precipitation from the WRF model at 3-km resolution. Zhang et al. (2018) found sensitivity to microphysics scheme and topographic height for their ability to reproduce observed rainfall. A WRF-based multi-physics analysis of an extreme rainfall event over the Beijing area was studied by Zhu and Xue (2016). The authors found microphysics to play an important part in peak rainfall intensity. Zhu and Xue (2016) studied combinations of microphysics, cumulus and radiation schemes with the radiation schemes having the least impact on rainfall.

Specific to solar forecasting, there are some studies that have attempted to conduct sensitivity analyses for one or more important parameterization options in WRF. Specifically, De Meij et al. (2018) analysed combinations of microphysics, cumulus and land-surface schemes for solar in Reunion Island. De Meij et al. (2018) used a single RTM model and found microphysics to have the largest impact on performance from the combinations tested. For Turkey, Incecik et al. (2019) analysed the performance of various microphysics and RTM options in WRF for forecasting surface irradiance. Incecik et al. (2019) found the choice of RTM to have the greatest impact on sunny days while there was no clear stand-out for partly cloudy days. However, with respect to solar irradiance, the authors are not aware of any study that attempts to systematically analyse the choice of surface schemes (surface layer physics, land surface model, planetary boundary layer [PBL] model), as well as RTM, microphysics and cumulus schemes. The choice of surface schemes may influence the development of cloud processes—in particular, shallow clouds. RTM clearly impacts the GHI values as surface irradiance is not

explicitly resolved by NWP models, but rather derived from an RTM scheme. Furthermore, the choices that relate to cloud processes including microphysics and cumulus parameterization should be considered for any optimization relating to surface irradiance. We propose that the surface, PBL, RTM and cloud/microphysics schemes be systematically tested to determine the combination that performs best under not just sunny, but also partly cloudy and cloudy conditions.

In the present study, we systematically test combinations of surface schemes with PBL options and then RTM with microphysics and cumulus schemes to determine the optimum configuration of the WRF model for a location in Qinghai, China. We then explore the use of adaptive WRF physics to improve the forecast of day-ahead solar irradiance for Qinghai, China. By changing the configuration of the model based on the global model forecast of irradiance, we show that overall WRF performance can be improved. The rest of the study is structured as follows: Section 2 describes the methods and observations, Section 3 presents the results (both physics optimization and then physics combinations), while Section 4 concludes the study and suggests future work arising from the results.

2 | EXPERIMENTAL METHODS

2.1 | Observations

The study period examined covers the dates from the years 2018 to 2019. Dates from 2018 were used to optimize the WRF model configuration, and the first 3 months of 2019 were used to validate the results. We considered global horizontal irradiance (GHI) observations from one location in Qinghai, China. The observation frequency is 15 min and we compared these values with output from the NWP model at the same frequency. As the observations represent a single local point in space, we also only extracted the nearest single point from our NWP domain (d01 from Figure 1b), to compare like-for-like. The study location is in the centre of the WRF domain to reduce the influence of interpolation at the model domain boundary.

2.2 | Numerical weather prediction

For the purposes of physically modelling the atmosphere over a limited area at high resolution, the most common and widely used NWP model is the WRF model. Although there are other options that exist and could be adapted to forecast for the Qinghai region, the WRF model is arguably the best choice given the active research community that continuously updates the model. The WRF model was developed by the collaboration of National Oceanographic and Atmospheric Administration (NOAA), the National Centre for Environmental Prediction (NCEP) and the National Centre for Atmospheric Research (NCAR) (Skamarock & Klemp, 2008), and at the time of this writing, the model has been updated up to version 4.2. We utilized the WRF model version 3.9.1 with initial and boundary conditions provided by the European Centre for Medium-Range Weather Forecasting (ECMWF), and we used the 1200 UTC release for all experiments. ECMWF model inputs were provided at a 3-hourly interval and with spatial resolution of roughly 0.1°. The WRF model was set up within the ECMWF model grid with one domain at 3 km spatial resolution and with 65 vertical layers. We forecasted for 52 h from each 1200 UTC release and utilized the day-

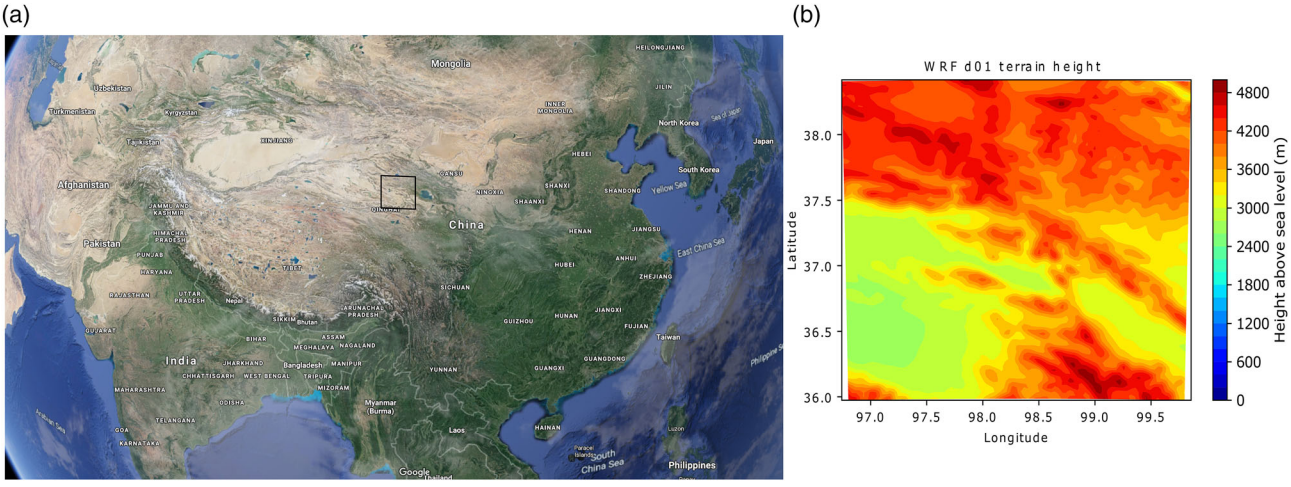

FIGURE 1 Qinghai region of China showing the area of study outlined in black in (a). WRF domain configuration with horizontal resolution at 3 km (d01 defined by the edge of the plotting area) showing model terrain height in (b). Background image re-appropriated from Google maps in (a). WRF, weather research and forecasting

ahead hours of +28 to +52 h, which correspond to midnight to midnight local time in Qinghai. The forecast period was chosen based on state grid requirements, which dictate that day-ahead forecasts be issued by 8 AM local time for the next day. In this way, the 1200 UTC model run, including delays in receiving the data and in running the model, is the most reliable and recent initialization time, which leads to the +28 to +52 h forecast horizon.

2.3 | WRF physics options

In Qinghai, China, Che et al. (2019) found small differences in root mean square error (RMSE) based solely on the choice of RTM with the Dudhia scheme, performing the best overall (a very similar result to Zempila et al., 2016). Nevertheless, it is important to consider various RTMs, because the RTM is entirely responsible for the GHI calculation within WRF. Parameterizations that directly impact cloud formation and cloud type should also be considered in order to find schemes that can most appropriately represent the cloudy processes at the location of choice. The schemes that estimate cloud particle concentration (microphysics) and the movement of these cloud properties through convective processes (cumulus schemes) should be optimized. Other important considerations may also involve the parameterization of surface processes. Specifically, those processes relate to the exchange of moisture and energy from the surface (surface physics and land-surface model), as well as the upward mixing of the atmosphere due to the roughness of the surface (PBL). We first evaluated the impact of the surface and PBL schemes on the performance of WRF day-ahead forecast of GHI. The surface and PBL schemes utilized are listed in Tables S1–S3 of the Supporting Information. A total of 179 combinations were tested (less than the complete set of combinations due mostly to incompatibility of schemes, but also due to computation constraints).

During testing of the surface and PBL schemes, the RTM, microphysics and cumulus parameterizations were kept constant with RRTMG long-wave, Dudhia short-wave, Thompson microphysics and no cumulus parameterization.

The options tested for RTM, microphysics and cumulus parameterization are outlined in Tables S4–S6 of the Supporting Information. During testing of these schemes, the surface and PBL schemes were kept constant at the optimum configuration found from the surface and PBL testing (NCEP Global Forecast System scheme, Rapid Update Cycle (RUC) land surface model and UW [Park and Bretherton] PBL scheme). A total of 160 combinations were run with 120 successfully simulating all days and subsequently being analysed. The configurations failing to complete all runs involved the Fu-Liou-Gu RTM schemes, and the failures were assumed to be due to numerical instability for the dates/region chosen.

With respect to the RTM schemes, the long-wave version of those listed in Table S6 of the Supporting Information were used, with the exception of the Dudhia short-wave, which has no long-wave counterpart, and so the RRTMG long-wave scheme was utilized instead. In order to decide which cumulus schemes to use, preference was given to the schemes that had some scale-awareness. At 3-km horizontal resolution, it is generally considered unnecessary to use cumulus physics, because convective processes start to become explicitly resolved by the model. Other options that relate to cloud processes and their relationship to radiation that were tested include sub-grid scale cloud interaction (cu_rad_feedback in WRF), which is available and was turned on for Grell and Kain–Fritsch cumulus schemes, cloud effects on optical depth (icloud in WRF), which is available and turned on for Dudhia and RRTMG-based RTM models, and feedback from shallow cumulus to the RTM (shallow_cu_fored_ra in WRF), which is available for Kain–Fritsch based cumulus schemes and was used with the default binning (21 bins) of potential temperature and mixing ratio.

2.4 | Sky condition characterization

Classification of sky cover amount was used in the present study to identify suitable optimization dates and the process of selecting WRF configurations in the validation period. Sky cover amount, k_t, is calculated by dividing the observed or modelled irradiance by the theoretical clear-sky irradiance as follows:

$$k_t(t) = \frac{I_{\text{observed}}(t)}{I_{\text{clearsky}}(t)}, \tag{1}$$

where I_{observed} is the observed or modelled irradiance for the Qinghai site, and I_{clearsky} is the theoretical clear-sky irradiance as calculated by the default Ineichen/Perez model from the python package pvlib. Observed irradiance was used in the training/optimization period, whereas the modelled irradiance, via the ECMWF model, was used to decide the WRF configuration for each day in the validation period.

2.5 | Measuring forecast accuracy

WRF SWDOWN (short-wave GHI) and ECMWF model SSRD (surface solar radiation downwards) values were compared with the observations via two measures: RMSE and bias. These measures are defined below:

$$\mathrm{RMSE} = \sqrt{\frac{1}{N}\sum \left(I_{\mathrm{pred}} - I_{\mathrm{obs}}\right)^2}, \tag{2}$$

$$\mathrm{Bias} = \frac{1}{N}\sum \left(I_{\mathrm{pred}} - I_{\mathrm{obs}}\right), \tag{3}$$

where I_{pred} is the WRF/ECMWF predicted irradiance (GHI) and I_{obs} is the measured GHI at the Qinghai site. The metrics were calculated at 15-min frequency of the observations. Irradiance values were determined by the WRF model RTMs at 3-min frequency but only the 15-min values starting on the hour were analysed in accordance with the observations. ECMWF model irradiance values are 3-hourly accumulated by the model from initialization and in units of J/m^2, which required deconstructing before comparing to the observations. Average W/m^2 values from each 3-h window were calculated by dividing with number of seconds in 3 h, which was done for both ECMWF model and 3-hourly accumulated clear-sky model values. Average k_t values were then calculated following Equation (1) and a linear interpolation performed in k_t-space to achieve 15-min k_t values. Finally, 15-min ECMWF model GHI values were extracted by multiplying with the 15-min frequency clear-sky model values. Night-time values were determined to be when the observations were equal to zero, and these times were not included in the RMSE and bias calculations.

2.6 | Choosing WRF configuration

WRF configuration options were tested on a representative 15-day period. The 15-day period was chosen based on daily-averaged k_t values from the observations with the intention of choosing five sunny days, five partly cloudy days and five cloudy days from across the year of 2018—akin to a typical meteorological year (TMY), but only for irradiance. To avoid spurious values for k_t, which are common near sunrise and sunset, only values with a solar zenith less than 70 degrees were included in the daily-average calculation. To decide which 15 days to use, we first split the daily-average values from 2018 into 15 bins of equal weight and based on increasing value. The first five bins were considered to represent cloudy days, the next five bins represent partly cloudy and the final five bins represent sunny days. From each bin a date was chosen and, where possible, choices were made to maximize the representation from across the year. The bins and the days chosen for each bin are outlined in Table 1. The corresponding time-series plot of the chosen dates is shown in Figure 2.

During the validation period, the decision of which WRF configuration to use was based on the forecast of

TABLE 1 Daily-average k_t binning, where the maximum value defines the upper limit of the bin, as well as the date chosen with the corresponding k_t value for each bin

Bin no.	1	2	3	4	5	6	7	8	9	10	11	12	13	14	15
Maximum k_t	0.32	0.44	0.53	0.59	0.66	0.69	0.73	0.78	0.82	0.85	0.88	0.93	0.96	0.99	1.09
Date chosen	2018-08-26	2018-03-05	2018-05-29	2018-09-11	2018-08-29	2018-03-28	2018-11-03	2018-04-30	2018-11-13	2018-10-17	2018-11-11	2018-09-22	2018-10-25	2018-11-12	2018-10-28
Date k_t	0.14	0.35	0.45	0.54	0.61	0.67	0.70	0.74	0.79	0.84	0.87	0.91	0.96	0.98	1.01

Notes: Dates are in local time.

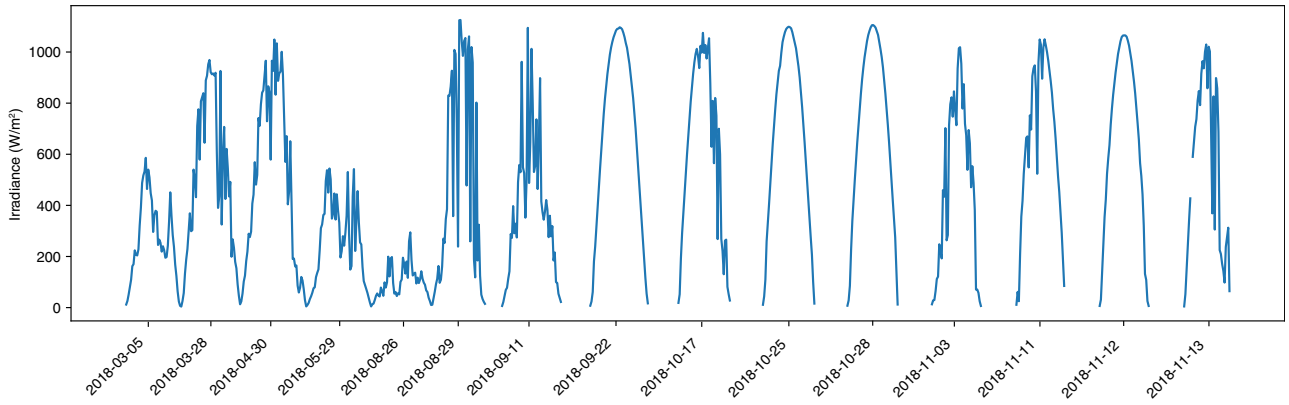

FIGURE 2 Time series of dates used in the optimization. Night-time values not plotted for brevity. Date stamps indicate the date in local time (UTC + 8 h)

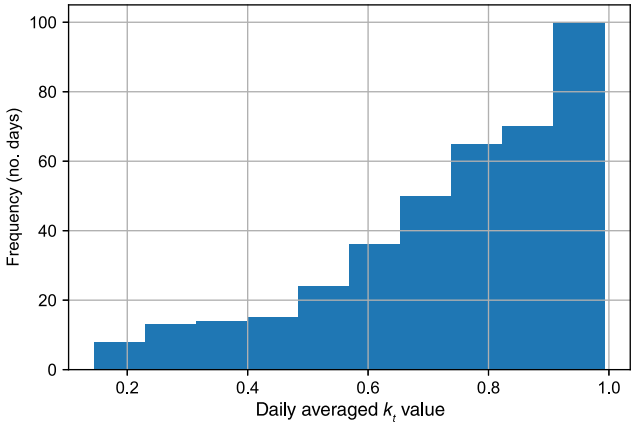

FIGURE 3 Distribution of daily-averaged k_t values for the ECMWF model in 2018. ECMWF, European Centre for Medium-Range Weather Forecasting

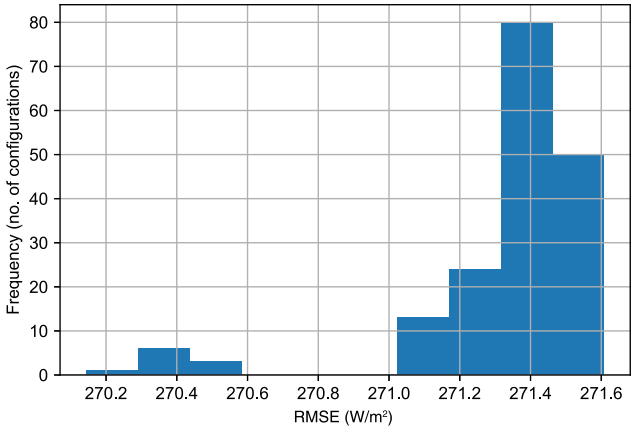

FIGURE 4 Histogram of RMSE performance for all 15 days and for all 179 surface and PBL scheme combinations tested in the study. PBL, planetary boundary layer; RMSE, root mean square error

irradiance from the ECMWF model. A priori the type of day based on observations is not known and the decision based on ECMWF model prediction was used in order for the method to be feasible in a true forecast setting. A similar process of binning was used for ECMWF model output; however, only three bins were used to determine the three cloud-amount categories. Further, the bins were adjusted due to the heavy bias on sunny days by the ECMWF model (Figure 3). The minimum value needed for a sunny day category from ECMWF was adjusted down to 0.915 from 0.933, and the minimum for a partly cloudy day was adjusted down to 0.753 from 0.783, based on a visual analysis of days near the boundary between categories (not shown). In the validation period, if the ECMWF model forecasted a sunny day then the sunny WRF physics were used, and so on for each category.

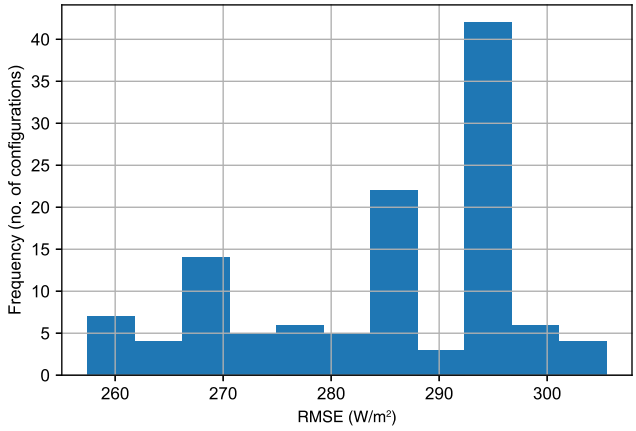

FIGURE 5 Histogram of RMSE performance for the RTM, microphysics and cumulus optimization using all 15 test period days. RMSE, root mean square error; RTM, radiative transfer model

3 | RESULTS AND DISCUSSION

The following result sections outline the results of the WRF physics optimization on a representative set of

15 days, as well as the implementation of adaptive WRF physics in a 3-month validation period (January–March 2019). The surface and PBL physics optimization was conducted first, followed by the RTM, microphysics and cumulus optimization. Analysis was then conducted based on observed type of day (sunny, partly cloudy and cloudy).

3.1 | Surface schemes and PBL optimization

The histogram of the results based on RMSE, for the 179 combinations tested, and using all 15 days is outlined in Figure 4. As can be seen from Figure 4, there is very little dependence on the surface or PBL schemes for the performance of WRF day-ahead forecast of GHI. The difference between best- and worst-performing combination was 0.5% based on RMSE. The small cluster centred on about 270.3 W/m^2 involved all except one of the combinations of NCEP Global Forecast System surface layer scheme and either RUC or 5-layer thermal diffusion land surface model. Realistically, for the Qinghai site, it seems that any of the tested combinations of surface and PBL schemes could be used without expecting the choice to influence performance. Nevertheless, for the rest of the results section, the optimum combination of NCEP Global Forecast System surface layer scheme, RUC land surface model and UW (Park and Bretherton) PBL scheme were utilized.

3.2 | RTM, microphysics and cumulus optimization

Figure 5 shows the histogram of RMSE based on all 15 days and for all combinations of RTM, microphysics and cumulus parameterization schemes that successfully completed all simulation days. A total of 120 schemes are included in Figure 5. Compared with the surface and PBL optimization, the RTM, microphysics and cumulus combinations show much more variability in performance. It should be noted that the cluster of combinations at around 295 W/m^2 RMSE all involved the use of the CAM RTM model, which appears inappropriate for this site. The top performing combination from optimization using all 15 test period days is outlined in Table 2.

3.2.1 | Optimization based on type of day

This section tests the hypothesis that the optimum WRF configuration has dependency on the type of day. The

TABLE 2 Top overall weather research and forecasting (WRF) configuration using the 15-day test period

Scheme	mp_phsyics	cu_physics	cudt	shcu_physics	ra_lw_physics	ra_sw_physics	icloud	cu_rad_feedback	shallow_forced_ra	nbins	cu_diag	ishallow
Overall option	22	0	0	0	4	4	3	False	False	N/A	0	0
Sunny option	22	0	0	2	4	4	3	False	False	N/A	0	0
Partly cloudy option	14	10	5	0	4	1	3	True	True	21	0	0
Cloudy option	28	5	0	0	4	1	3	True	False	N/A	1	1

Notes: WRF name list options instead of full names are stated for brevity.

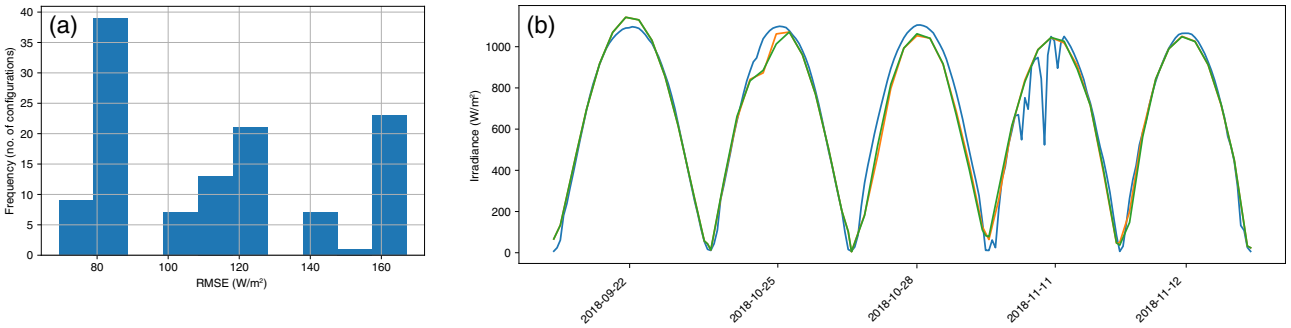

FIGURE 6 Histogram of results for the RTM, microphysics and cumulus combinations for sunny days in (a). Time-series plot of the optimum sunny configuration (orange) compared with the best overall configuration (green) and with the observations (blue) in (b). Observed night-time values are not plotted in (b) for ease of visualization. RTM, radiative transfer model

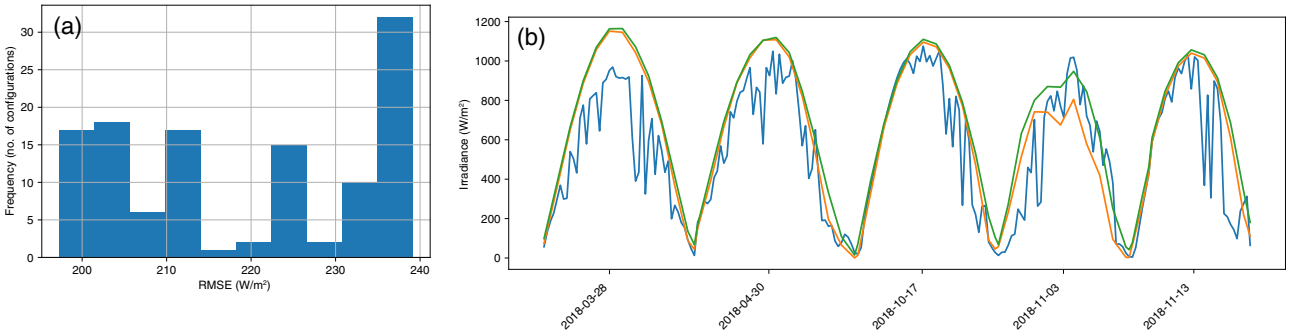

FIGURE 7 As per Figure 6 except for analysis carried out on partly cloudy days and where the best partly cloudy configuration is plotted with orange in (b)

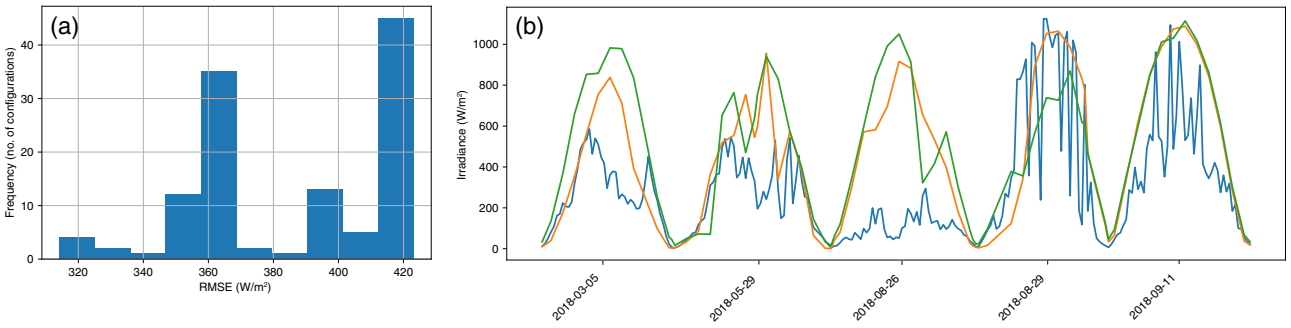

FIGURE 8 As per Figure 7 except for analysis carried out on cloudy days and where the best cloudy configuration is plotted with orange in (b)

basic assumption being that the physical options influencing cloud processes in WRF have a greater impact on GHI modelling for cloudy days when compared with sunny days. The difference is outlined by splitting the full set of 15 days into their respective sunny, partly cloudy and cloudy categories, running the RMSE analysis for each category and then analysing the top category-based physics option with the configuration found to work best overall. Figure 6a shows the histogram of RMSE performance for the RTM, microphysics and cumulus options for the five sunny days. Figure 6b shows the time-series plot comparing the best-performing sunny configuration with the best overall configuration for the five sunny days.

For sunny days, the difference between the best overall and the best sunny configuration was small at 69.2 W/m^2 for sunny option versus 70.02 W/m^2 for the best overall. The reason for the similarity can be traced back to the WRF configurations, which are almost identical (Table 2). Clustering in performance was evident for the

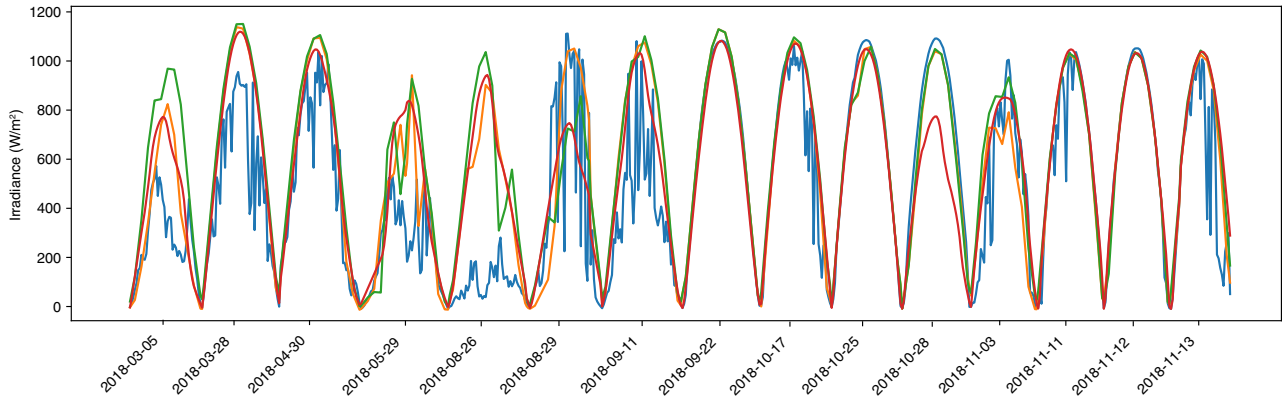

FIGURE 9 Time-series comparison between the best overall configuration (green), the ECMWF model (red) and the combined WRF output (orange), which represent the concatenation of optimum configurations based on their respective day category. Observations are plotted in blue. ECMWF, European Centre for Medium-Range Weather Forecasting; WRF, weather research and forecasting

TABLE 3 Statistics using all 15 days, where combined WRF represents the concatenation of optimum sunny, partly cloudy and cloudy configurations for their respective days

Model	RMSE (W/m^2)	Bias (W/m^2)
Combined WRF	222.51	90.13
Overall WRF	257.46	124.19
ECMWF model	231.77	81.75

Abbreviations: ECMWF, European Centre for Medium-Range Weather Forecasting; RMSE, root mean square error; WRF, weather research and forecasting.

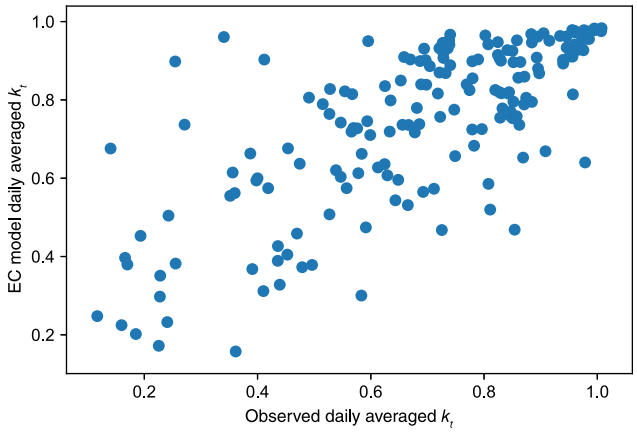

FIGURE 10 Scatter plot comparing ECMWF and observed daily-averaged k_t values for 2018. ECMWF, European Centre for Medium-Range Weather Forecasting

sunny days. Figure 6a shows that there were three distinct clusters. The difference between the first cluster at around 80 W/m^2 and the second cluster beyond 100 W/m^2 occurred when switching to Thompson microphysics with RRTMG long-wave and short-wave schemes in conjunction with certain cumulus options. The jump in performance from cluster two to cluster three was for similar reasons but with Dudhia short-wave scheme instead of RRTMG.

For partly cloudy days, the difference was more marked, although most of the difference was due to one of the 5 days. Cumulus physics was preferred for partly cloudy days (Table 2) arising in a more accurate representation of the cloud amount on day 4 (the second cloudiest from the partly cloudy category) (Figure 7). The RMSE for the best partly cloudy configuration on partly cloudy days was 197.31 W/m^2 compared with 214.49 W/m^2 for the best overall configuration on the same days.

During the optimization period, by far the biggest difference between choosing the overall best WRF configuration versus a configuration chosen based on day type was for the cloudy category. Cumulus physics were also preferred for the cloudy category (Table 2) and the difference in RMSE was 15.7% when comparing the best cloudy configuration (314.29 W/m^2) with the best overall (372.9 W/m^2). Figure 8b shows that this difference is also much more visible in the time series across nearly all 5 days. Some clustering in performance is also visible for the cloudy category (Figure 8a). The first cluster in performance (at around 360 W/m^2) for cloudy days was due to the configurations using RRTMG long-wave and Dudhia short-wave RTMs, while the second cluster (at around 420 W/m^2) was centred on the configurations using the CAM RTM.

Given that there was a difference in performance when the WRF RTM, microphysics and cumulus options were tailored for the type of day it then follows that overall the best choice is to utilize day-type-specific WRF configurations. For the 15-day test period, when the optimum configuration for each day type was chosen, not only was the overall RMSE lower than choosing the best

TABLE 4 As per Table 3 but for the 3-month validation set

Model	Overall RMSE (W/m^2)	Overall bias (W/m^2)	Sunny RMSE (W/m^2)	Sunny bias (W/m^2)	Partly cloudy RMSE (W/m^2)	Partly cloudy bias (W/m^2)	Cloudy RMSE (W/m^2)	Cloudy bias (W/m^2)
Combined WRF	232.36	−59.15	185.77	−66.80	261.68	−90.26	250.80	−6.69
Overall WRF	282.83	−111.53	228.34	−92.65	330.51	−156.88	284.04	−78.0
ECMWF model	203.57	37.71	120.66	−12.93	213.41	20.77	277.67	132.68

Notes: Results are also presented based on the observed type of day.
Abbreviations: ECMWF, European Centre for Medium-Range Weather Forecasting; RMSE, root mean square error; WRF, weather research and forecasting.

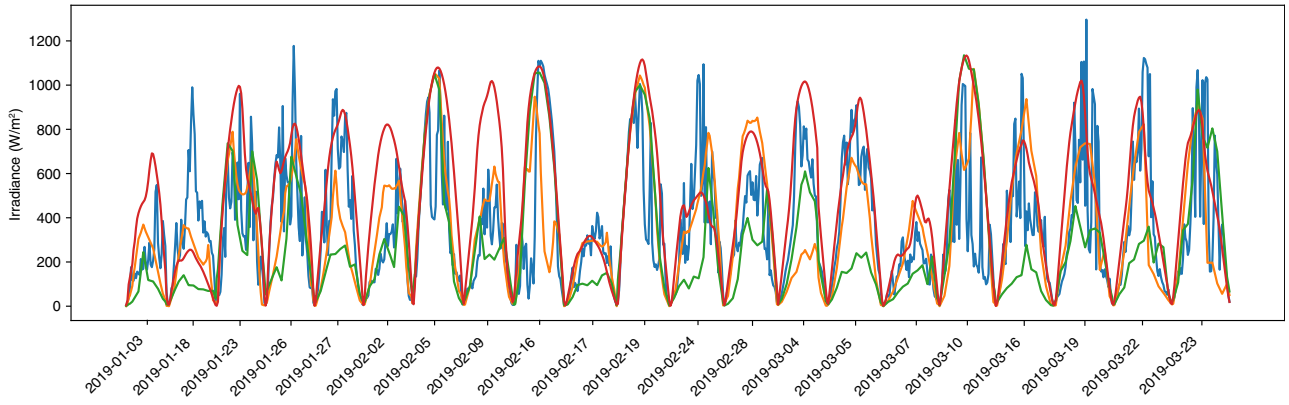

FIGURE 11 Time-series plot of observed cloudy days from validation set. The best overall configuration is in green, the ECMWF model in red, the combined WRF output in orange and the observations are plotted in blue. ECMWF, European Centre for Medium-Range Weather Forecasting; WRF, weather research and forecasting

overall configuration, but the RMSE was also lower than the ECMWF global model input. Figure 9 illustrates this difference for the 15-day time series while Table 3 states the RMSE and bias statistics for the 15-day optimization period.

3.3 | Adaptive WRF physics

Beyond the performance on the optimization set, the question of the benefit from implementing day-type physics requires longer examination on new data. As the observed day is not known a priori, we utilize the forecast from the ECMWF model in order to choose the WRF physics for each day in a 3-month validation set (January–March 2019). While this introduces a source of error as the ECMWF model forecast is not 100% accurate on the type of day, it is a practical choice. Figure 10 shows the scatter plot of ECMWF-derived daily-average k_t versus the observed daily-averaged k_t for 2018. There is a reasonable correlation at 0.746 between ECMWF model and observed daily-averaged cloud amount with an expected sunny bias from ECMWF.

For each day in the validation set, the ECMWF-derived categories for sunny, partly cloudy and cloudy were used to determine the physics for the WRF model. If the ECMWF model forecasted a sunny day then sunny WRF physics were used, and so on for the other two categories. The best overall WRF configuration was also run in parallel for each day for comparison. The resulting statistics are outlined in Table 4.

For the validation set, the use of adaptive physics is clearly superior than the use of a single WRF configuration. Both the RMSE and bias statistics are favourable for the use of adaptive WRF physics. While the ECMWF model out-performs the combined model during January–March 2019, this was dependent on the type of day and not true for the cloudy category. For cloudy days in January–March 2019, the use of adaptive physics remains better than a single WRF configuration, and with smaller error than the ECMWF model. Figure 11 shows the time series of January–March 2019 cloudy days based on the observed conditions. For cloudy days, it is evident that the overall best WRF configuration greatly over-predicts cloud amount with bias of −78 W/m^2 compared with the adaptive WRF configuration at −6.7 W/

m^2 and the ECMWF model at 132.68 W/m^2, which greatly over-predicts irradiance (Table 4).

The RMSE and bias statistics for the validation set split by day type are also outlined in Table 4. As can be seen from the day-type results, the adaptive physics was a better choice overall and for any type of the day, while the ECMWF model performance deteriorates with increasing cloud amount. For cloudy conditions, it is generally expected that limited-area physical downscaling produces better resolved clouds and cloud processes through tailored physics and higher resolution, and this is what we have found for the Qinghai site.

4 | CONCLUSIONS

In the present study, a comprehensive physics test was conducted for a location in Qinghai, China, and then adaptive physics, based on the forecast day type, was implemented. Using the WRF model at 3 km horizontal resolution and downscaling from the European Centre for Medium-Range Weather Forecasting (ECMWF) global model, parameterizations that control surface, planetary boundary layer (PBL), radiative transfer and cloud processes were systematically tested for the purposes of day-ahead global horizontal irradiance (GHI) forecasting. On a representative 15-day sample set, the surface and PBL schemes were first tested, followed by the radiative transfer model (RTM), microphysics and cumulus schemes. Surface and PBL schemes were found to have very little influence on the performance of day-ahead GHI forecasts for the Qinghai site (maximum difference of 0.5% root mean square error [RMSE]). RTM, microphysics and cumulus schemes, on the other hand, were shown to have a difference of 15.7% RMSE between the worst- and best-performing configuration.

Sensitivity to the type of day for the optimum WRF configuration was then conducted. The difference between the best overall configuration and the best configuration based on the type of day (sunny, partly cloudy and cloudy) was greatest on cloudy days. On cloudy and partly cloudy days cumulus schemes were preferred with no cumulus on sunny days. On the full optimization set, the choice of physics based on the type of day out-performed the best overall configuration and the ECMWF model by 13.5% and 4.2%, respectively.

Testing on a larger and new 3-month validation set was then conducted, and the ECMWF model forecast conditions were utilized to choose the physics for each day for the adaptive model. On the validation set, day-type physics continued to out-perform the best overall configuration with an increase in performance of 17.8% RMSE; however, the ECMWF model, which provides the data to drive the WRF model, performed best overall. Considering the performance on type of day, it was shown that increasing cloud gave rise to superior performance by the day-type WRF model. For cloudy days in the validation set, the version of WRF with physics adapted based on the ECMWF forecast out-performed the single best WRF configuration by 11.7% and the ECMWF model by 9.7%.

In the present study, we have shown that, where possible, the choice of WRF physics should be adapted to not only the location being forecasted but also the type of conditions. By using the global model as a guide for the type of day in the forecast period, the condition-specific WRF physics can be implemented and continue to outperform even the best static configuration. For this site, based on the work presented here, the best option for forecasting surface irradiance is the use of the ECMWF model for forecasted sunny and partly cloudy days and the cloudy WRF for forecasted cloudy days. Future work should consider using the superior WRF output as input to post-processing algorithms. Algorithms that are capable of utilizing other variables (i.e., temperature, wind speed, humidity, etc.) from the top performing model each day should help to further improve the performance. Further analysis of the corresponding improvement in photovoltaic power following from the lower GHI RMSE should also be considered.

ACKNOWLEDGEMENTS

The authors acknowledge Envision Group Pte Ltd for funding the research, the European Centre for Medium-Range Weather Forecasts for the data used to drive the WRF model and Tianhe-2 supercomputer where the simulations were run.

AUTHOR CONTRIBUTIONS

Robert Huva: Formal analysis (lead); investigation (lead); methodology (equal); visualization (lead); writing – original draft (lead); writing – review and editing (equal). **Guiting Song:** Conceptualization (lead); funding acquisition (lead); resources (lead); supervision (lead); writing – review and editing (equal). **Xiaohui Zhong:** Conceptualization (equal); methodology (equal); writing – review and editing (equal). **Yangyang Zhao:** Conceptualization (equal); methodology (equal); software (lead).

ORCID

Robert Huva https://orcid.org/0000-0003-3677-6524

REFERENCES

Australian Electricity Market Operator (AEMO). (2020) *Solar and wind energy forecasting system*. Available at: https://aemo.com.au/en/energy-systems/electricity/national-electricity-market-nem/

nem-forecasting-and-planning/operational-forecasting/solar-and-wind-energy-forecasting [Accessed 1st June 2020].

Ahmed, R., Sreeram, V., Mishra, Y. & Arif, M.D. (2020) A review and evaluation of the state-of-the-art in PV solar power forecasting: techniques and optimization. *Renewable and Sustainable Energy Reviews*, 124, 109792.

Che, Y., Chen, L., Zheng, J., Yuan, L. & Xiao, F. (2019) A novel hybrid model of WRF and clearness index-based kalman filter for day-ahead solar radiation forecasting. *Applied Sciences*, 9, 1–16.

China GB/T 19964-2012. (n.d.) *Technical requirements for connecting photovoltaic power stations to power systems, China*. Available at: https://www.chinesestandard.net/PDF.aspx/GBT19964-2012 [Accessed 1st June 2020].

De Meij, A., Vinuesa, J.F. & Maupas, V. (2018) GHI calculation sensitivity on microphysics, land- and cumulus parameterization in WRF over the Reunion Island. *Atmospheric Research*, 204, 12–20.

Diagne, M., David, M., Boland, J., Schmutz, N. & Lauret, P. (2014) Post-processing of solar irradiance forecasts from WRF model at Reunion Island. *Energy Procedia*, 57, 1364–1373.

Duan, H., Li, Y., Zhang, T., Pu, Z., Zhao, C. & Liu, Y. (2018) Evaluation of the forecast accuracy of near-surface temperature and wind in Northwest China based on the WRF model. *Journal of Meteorological Research*, 32, 469–490.

Huang, J. & Thatcher, M. (2017) Assessing the value of simulated regional weather variability in solar forecasting using numerical weather prediction. *Solar Energy*, 144, 529–539.

International Energy Agency (IEA). (2019) *Renewables Information 2019*. Available at: https://www.iea.org/reports/renewables-information-2019 [Accessed 1st June 2020].

Incecik, S., Sakarya, S., Tilev, S., Kahraman, A., Aksoy, B., Caliskan, E. et al. (2019) Evaluation of WRF parameterizations for global horizontal irradiation forecasts: a study for Turkey. *Atmosfera*, 32, 143–158.

Jimenez, P.A., Hacker, J.P., Dudhia, J., Haupt, S.E., Ruiz-Arias, J. A., Gueymard, C.A. et al. (2016) WRF-SOLAR: description and clear-sky assessment of an augmented NWP model for solar power prediction. *Bulletin of the American Meteorological Society*, 97, 1249–1264.

Larson, D.P., Nonnenmacher, L. & Coimbra, C.F.M. (2016) Day-ahead forecasting of solar power output from photovoltaic plants in the American southwest. *Renewable Energy*, 91, 11–20.

Mitra, I., Sharma, S., Kaur, M., Ramanan, A., Wypior, M. & Heinemann, D. (2016) Evolution of solar forecasting in India: the introduction of REMCs. *EuroSun 2016 Conference Proceedings, International Solar Energy Society*, pp. 1 1–10. http://proceedings.ises.org/paper/eurosun2016/eurosun2016-0165-Mitra.pdf.

Murata, A., Ohtake, H. & Oozeki, T. (2018) Modeling of uncertainty of solar irradiance forecasts on numerical weather predictions with the estimation of multiple confidence intervals. *Renewable Energy*, 117, 193–201.

Skamarock, W.C. & Klemp, J.B. (2008) A time-split nonhydrostatic atmospheric model for weather research and forecasting applications. *Journal of Computational Physics*, 227, 3465–3485.

Song, Y., Chen, G. & Wang, W.C. (2019) Aerosol direct radiative and cloud adjustment effects on surface climate over eastern China: analyses of WRF model simulations. *Journal of Climate*, 32, 1293–1306.

Verbois, H., Huva, R., Rusydi, A. & Walsh, W. (2018) Solar irradiance forecasting in the tropics using numerical weather prediction and statistical learning. *Solar Energy*, 162, 265–277.

Zempila, M.-M., Giannaros, T.M., Bais, A., Melas, D. & Kazantzidis, A. (2016) Evaluation of WRF shortwave radiation parameterizations in predicting global horizontal irradiance in Greece. *Renewable Energy*, 86, 831–840.

Zhang, X., Xiong, Z., Zheng, J. & Ge, Q. (2018) High-resolution precipitation data derived from dynamical downscaling using the WRF model for the Heihe River basin, Northwest China. *Theoretical and Applied Climatology*, 131, 1249–1259.

Zhu, K. & Xue, M. (2016) Evaluation of WRF-based convection-permitting multi-physics ensemble forecasts over China for an extreme rainfall event on 21 July 2012 in Beijing. *Advances in Atmospheric Sciences*, 33, 1240–1258.

REFERENCES CITED IN SUPPORTING INFORMATION

*Angevine, W.M., Jiang, H. & Mauritsen, T. (2010) Performance of an eddy diffusivity-mass flux scheme for shallow cumulus boundary layers. *Monthly Weather Review*, 138, 2895–2912.

*Beljaars, A.C.M. (1995) The parameterization of surface fluxes in large-scale models under free convection. *Quarterly Journal of the Royal Meteorological Society*, 121, 255–270.

*Benjamin, S., Bleck, R., Brown, J., Brundage, K., Devenyi, D., Grell, G., et al. (2004) Mesoscale weather prediction with the RUC hybrid isentropic-sigma coordinate model and data assimilation system operational numerical weather prediction. In: *Symposium on the 50th Anniversary of Operational Numerical Weather Prediction*, pp. 495–518.

*Berg, L.K., Gustafson, W.I., Kassianov, E.I. & Deng, L. (2013) Evaluation of a modified scheme for shallow convection: implementation of CuP and case studies. *Monthly Weather Review*, 141, 134–147.

*Bougeault, P. & Lacarrere, P. (1989) Parameterization of orography-induced turbulence in a mesobeta-scale model. *Monthly Weather Review*, 117, 1872–1890.

*Chen, J., Carlson, B.E. & Del Genio, A.D. (2002) Evidence for strengthening of the tropical general circulation in the 1990s. *Science*, 295, 838–841.

*Collins, W.D., Rasch, P.J.., Boville, B.A., Hack, J.J., Williamson, D. L., Kiehl, J.T., et al. (2004) *Description of the NCAR Community Atmosphere Model (CAM 3.0)*. Ncar/Tn-464+Str, pp. 214.

*Dudhia, J. (1989) Numerical study of convection observed during the winter monsoon experiment using a mesoscale two-dimensional model. *Journal of the Atmospheric Sciences*, 46, 3077–3107.

*Dudhia, J. (1996) A multi-layer soil temperature model for MM5. In: *The sixth PSU/NCAR mesoscale model users' workshop*.

*Glotfelty, T., Alapaty, K., He, J., Hawbecker, P., Song, X. & Zhang, G. (2019) The weather research and forecasting model with aerosol-cloud interactions (WRF-ACI): development, evaluation, and initial application. *Monthly Weather Review*, 147, 1491–1511.

*Grell, G.A. & Dévényi, D. (2002) A generalized approach to parameterizing convection combining ensemble and data assimilation techniques. *Geophysical Research Letters*, 29, 10–13.

*Grell, G.A. & Freitas, S.R. (2013) A scale and aerosol aware stochastic convective parameterization for weather and air quality modeling. *Atmospheric Chemistry and Physics Discussions*, 13, 23845–23893.

*Grenier, H. & Bretherton, C.S. (2001) A moist PBL parameterization for large-scale models and its application to subtropical cloud-topped marine boundary layers. *Monthly Weather Review*, 129, 357–377.

*Gu, Y., Liou, K.N., Ou, S.C. & Fovell, R. (2011) Cirrus cloud simulations using WRF with improved radiation parameterization and increased vertical resolution. *Journal of Geophysical Research—Atmospheres*, 116, 1–14.

*Hong, S.Y. & Jang, J. (2018) Impacts of shallow convection processes on a simulated boreal summer climatology in a global atmospheric model. *Asia-Pacific Journal of Atmospheric Sciences*, 54, 361–370.

*Hong, S.Y. & Pan, H.L. (1996) Nonlocal boundary layer vertical diffusion in a medium-range forecast model. *Monthly Weather Review*, 124, 2322–2339.

*Hong, S.Y., Noh, Y. & Dudhia, J. (2006) A new vertical diffusion package with an explicit treatment of entrainment processes. *Monthly Weather Review*, 134, 2318–2341.

*Iacono, M.J., Delamere, J.S., Mlawer, E.J., Shephard, M.W., Clough, S.A. & Collins, W.D. (2008) Radiative forcing by long-lived greenhouse gases: calculations with the AER radiative transfer models. *Journal of Geophysical Research—Atmospheres*, 113, 2–9.

*Janjic, Z.I. (1994) The step-mountain eta coordinate model: further developments of the convection, viscous sublayer, and turbulence closure schemes. *Monthly Weather Review*, 122, 927–945.

*Jiménez, P.A., Dudhia, J., González-Rouco, J.F., Navarro, J., Montávez, J.P. & García-Bustamante, E. (2012) A revised scheme for the WRF surface layer formulation. *Monthly Weather Review*, 140, 898–918.

*Kain, J.S. & Kain, J. (2004) The Kain–Fritsch convective parameterization: an update. *Journal of Applied Meteorology*, 43, 170–181.

*Lim, K.S.S. & Hong, S.Y. (2010) Development of an effective double-moment cloud microphysics scheme with prognostic cloud condensation nuclei (CCN) for weather and climate models. *Monthly Weather Review*, 138, 1587–1612.

*Mansell, E.R., Ziegler, C.L. & Bruning, E.C. (2010) Simulated electrification of a small thunderstorm with two-moment bulk microphysics. *Journal of the Atmospheric Sciences*, 67, 171–194.

*Nakanishi, M. & Niino, H. (2006) An improved Mellor-Yamada Level-3 model: its numerical stability and application to a regional prediction of advection fog. *Boundary-Layer Meteorology*, 119, 397–407.

*Niu, G.Y., Yang, Z.L., Mitchell, K.E., Chen, F., Ek, M.B., Barlage, M. et al. (2011) The community Noah land surface model with multiparameterization options (Noah-MP): 1. Model description and evaluation with local-scale measurements. *Journal of Geophysical Research: Atmospheres*, 116, 1–19.

*Park, S. & Bretherton, C.S. (2009) The University of Washington shallow convection and moist turbulence schemes and their impact on climate simulations with the community atmosphere model. *Journal of Climate*, 22, 3449–3469.

*Pleim, J.E. (2006) A simple, efficient solution of flux–profile relationships in the atmospheric surface layer. *Journal of Applied Meteorology and Climatology*, 45, 341–347.

*Pleim, J.E. (2007) A combined local and nonlocal closure model for the atmospheric boundary layer. Part I: model description and testing. *Journal of Applied Meteorology and Climatology*, 46, 1383–1395.

*Shin, H.H. & Hong, S.Y. (2015) Representation of the subgrid-scale turbulent transport in convective boundary layers at gray-zone resolutions. *Monthly Weather Review*, 143, 250–271.

*Sukoriansky, S., Galperin, B. & Perov, V. (2005) Application of a new spectral theory of stably stratified turbulence to the atmospheric boundary layer over sea ice. *Boundary-Layer Meteorology*, 117, 231–257.

*Tewari, M., Chen, F., Wang, W., Dudhia, J., LeMone, M.A., Mitchel, K. et al. (2004) Implementation and verification of the unified NOAH land surface model in the WRF model. In: *20th conference on weather analysis and forecasting/16th conference on numerical weather prediction*, pp. 11–15.

*Thompson, G. & Eidhammer, T. (2014) A study of aerosol impacts on clouds and precipitation development in a large winter cyclone. *Journal of the Atmospheric Sciences*, 71, 3636–3658.

*Xiu, A. & Pleim, J.E. (2001) Development of a land surface model. Part I: application in a mesoscale meteorological model. *Journal of Applied Meteorology and Climatology*, 40, 192–209.

SUPPORTING INFORMATION

Additional supporting information may be found online in the Supporting Information section at the end of this article.

How to cite this article: Huva, R., Song, G., Zhong, X., & Zhao, Y. (2021). Comprehensive physics testing and adaptive weather research and forecasting physics for day-ahead solar forecasting. *Meteorological Applications*, *28*(4), e2017. https://doi.org/10.1002/met.2017